Mechanics of Materials 9 (1990) 139–163
Elsevier

MODELS OF FIBER DEBONDING AND PULLOUT IN BRITTLE COMPOSITES WITH FRICTION

John W. HUTCHINSON

Division of Applied Sciences, Harvard University, Cambridge MA 02138, U.S.A.

Henrik M. JENSEN

Department of Solid Mechanics, The Technical University of Denmark, DK-2800 Lyngby, Denmark

Received 12 March 1990

Models for the debonding of a fiber embedded in a brittle matrix are proposed and analyzed. Attention is restricted to systems having a residual compressive stress acting across the fiber/matrix interface. Debonding, as well as pullout after the fiber breaks, is accompanied by frictional sliding. Fiber–matrix interaction is modeled by a cylindrical cell with two sets of boundary conditions: one modeling an isolated fiber–matrix unit and the other a matrix containing an array of unidirectional fibers. The elastic properties of the fiber are taken to be transversely isotropic about the fiber axis, while the matrix is assumed to be isotropic. The debonding process is treated within the framework of fracture mechanics as a mode 2 crack. Two idealizations of friction are considered: a constant friction stress independent of normal compression across the interface, and Coulomb friction. Approximate closed form solutions to the model are presented. These are assessed using results from an accurate numerical analysis.

Notation (Partial listing)

a_i, b_i, c_i	nondimensional coefficients – Appendix B
E_f, E_m	moduli of fiber and matrix
$\mathscr{G}$	energy release rate of debond crack
$\mathscr{G}_c$	mode 2 toughness
$\mathscr{G}_c^*$	maximum value of $\mathscr{G}_c$ for mode 2 debonding
l, l_0	debond lengths – Fig. 2
R	radius of cylindrical cell
R_f	radius of fiber
δ	displacement between end of fiber and matrix – Fig. 2
Δ	additional displacement due to debonding – see (16) and (38)
ϵ_f, ϵ_m	axial strains in fiber and matrix
ϵ_r^T, ϵ_z^T	radial and axial mismatch strains of fiber – see (1) and (2)
$\epsilon^T \equiv \epsilon_z^T$	
ν_m	Poisson's ratio of matrix
ν_f, ζ_f	ratios of transversely isotropic fiber – see (2)
$\lambda = \epsilon_r^T/\epsilon_z^T$	
μ	coefficient of friction
$\rho = (R_f/R)^2$	area fraction of fiber
σ_f, σ_m	axial stresses in fiber and matrix
σ_r	radial component of stress at interface (unless otherwise stated)

$\bar{\sigma}$	average axial stress
$\bar{\sigma}_i$	$\bar{\sigma}$ at initiation of bond
$\bar{\sigma}_c$	$\bar{\sigma}$ at fiber break
$\bar{\sigma}_b$	$\bar{\sigma}$ just after fiber break
$\bar{\sigma}_0$	maximum value of $\bar{\sigma}$ – see (9) and (26)

1. Introduction

1.1. Background and organization of the paper

Enhanced toughness of a ceramic matrix composite reinforced by ceramic fibers requires that a matrix crack traversing the composite leave uncracked fibers behind its front to provide bridging restraint across the crack. For this to occur, the toughness of the fiber/matrix interface must be sufficiently low relative to the toughness of the fiber such that the matrix crack induces fiber debonding rather than fiber cracking as it engulfs the fiber. If debonding is initiated, the toughness enhancement of the composite depends on the extent of debonding before the fiber breaks and the work dissipated by friction during pullout, as discussed in the review articles by Evans (1989) and Thouless et al. (1989). Friction effects will be most important in systems which have a residual compressive stress acting across the fiber/matrix interface. If the friction is too large the extent of the debond will be small when the fiber breaks and the energy dissipated due to debonding and pullout will be limited. Conversely, if the level of friction is too small, the extent of the debond will tend to be large but the pullout work will also be small. This suggests the existence of an optimal friction level to maximize the toughness enhancement, but how this level depends on the residual stresses, the elastic properties of the fiber and matrix, and the toughness of the interface bond has not yet been established. The models presented in this paper are intended for this purpose, as well as supplying a mechanics analysis for the experimental determination of interfacial toughness and friction.

The correct characterization of frictional sliding of a fiber embedded in a matrix remains an open issue. Fiber push-out tests (Marshall and Oliver, 1987; Bright et al., 1989) have been designed to directly measure friction stresses. Theoretical models, guided by the experimental findings, have usually assumed either a constant friction stress, presumably due to asperities, or Coulomb friction. Both characterizations are considered in this paper.

The present study is confined to systems which have a residual compressive stress acting across the fiber/matrix interface of the unloaded composite. Axisymmetric cylindrical models such as those shown in Figs. 1 and 2 are analyzed. Cylindrical models of this type have been considered previously by a number of workers. Wells and Beaumont (1985) review some of the earlier studies preliminary to their own modeling. The present study is most closely related to those of Gao et al. (1988) and Sigl and Evans (1989) who also considered the role of friction and residual compressive stress across the interface. The study by Charalambides and Evans (1989) complements the present work in that it deals with fiber debonding when the residual stress across the interface is tensile such that the debond crack is open and friction-free.

Debonding is viewed as mode 2 interface fracture and is treated by a fracture mechanics approach. Two characterizations of sliding friction are considered: (1) a constant friction stress τ over all portions of the interface experiencing compressive normal stress σ_r and (2) Coulomb friction with $\tau = -\mu\sigma_r$ where σ_r is negative. The matrix material is taken to be elastic and isotropic with Young's modulus E_m and Poisson's ratio ν_m. The fiber is taken to be transversely isotropic with respect to its cylindrical axis. Let ϵ_r^T and ϵ_z^T be the mismatch strains between the fiber and matrix in the sense that the free-standing fiber is too "fat" and "long" for the unstressed matrix as measured by ϵ_r^T and ϵ_z^T.

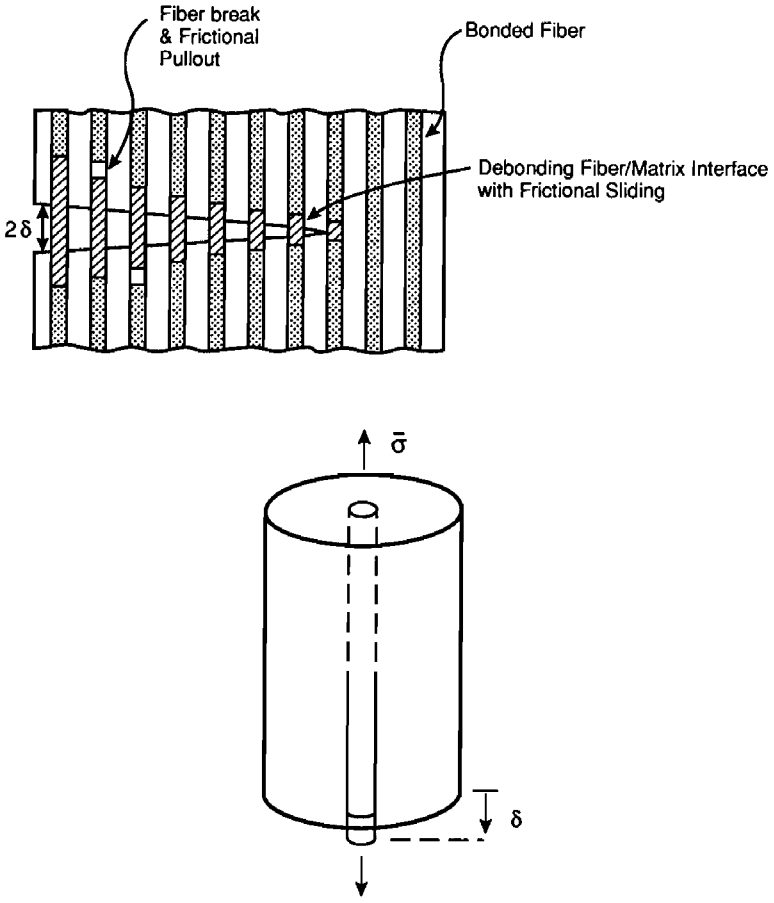

Fig. 1. Schematic of fiber debonding and pullout behind a matrix crack. Axisymmetric cylindrical cell model with two types of boundary conditions: Type I = zero tractions modeling a single fiber–matrix unit, Type II = zero shear traction with constrained normal displacement modeling a doubly periodic array of fibers.

If the fiber, and the matrix hole into which it fits, is imagined to be perfectly uniform and if misfit strains are due to thermal expansion mismatch, then

$$\epsilon_r^{\mathrm{T}} = \int_0^{\Delta T} \left(\alpha_r^f - \alpha^m\right) \mathrm{d}T, \quad \epsilon_z^{\mathrm{T}} = \int_0^{\Delta T} \left(\alpha_z^{\mathrm{f}} - \alpha^{\mathrm{m}}\right) \mathrm{d}T, \tag{1}$$

where ΔT is the temperature change from bonding, and the coefficients of thermal expansion are α^{m} for the matrix and α_r^{f} and α_z^{f} in the radial and axial directions for the fiber. Mismatch can also arise from nonuniformity in the fiber. For example, if there is a variation in the radius of the fiber along its length of magnitude ΔR_{f}, there will be a radial misfit strain proportional to $\Delta R_{\mathrm{f}}/R_{\mathrm{f}}$ after the fiber has slipped some distance. The mechanics of the misfit arising from this source has not yet been worked out.

Thus, with the misfit strains taken to be associated with the fiber, the general relation between strains and stresses in a transversely isotropic fiber undergoing axisymmetric deformation (with $\sigma_\theta = \sigma_r$ and $\epsilon_\theta = \epsilon_r$) can be written as

$$\begin{aligned} E_{\mathrm{f}}\left(\epsilon_z - \epsilon_z^{\mathrm{T}}\right) &= \sigma_z - 2\nu_{\mathrm{f}}\sigma_r, \\ E_{\mathrm{f}}\left(\epsilon_r - \epsilon_r^{\mathrm{T}}\right) &= \zeta_{\mathrm{f}}\sigma_r - \nu_{\mathrm{f}}\sigma_z. \end{aligned} \tag{2}$$

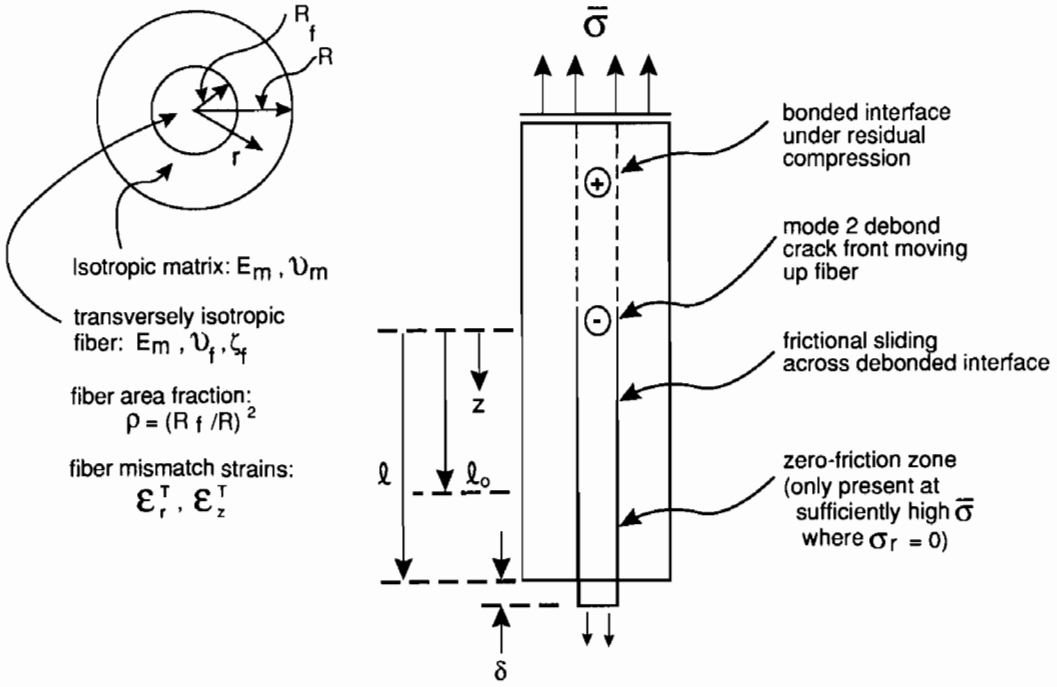

Fig. 2. Conventions and definitions for cylindrical models.

When the fiber is isotropic, $\zeta_f = 1 - \nu_f$. When it is not, $\zeta_f = (1 - \nu_r)(E_f/E_r)$ where ν_r and E_r are the Poisson's ratio and Young's modulus governing behavior in the plane perpendicular to the fiber axis. The relation for the matrix under axisymmetric deformation is

$$\begin{aligned} E_m\epsilon_z &= \sigma_z - \nu_m(\sigma_r + \sigma_\theta) \\ E_m\epsilon_r &= \sigma_r - \nu_m(\sigma_\theta + \sigma_z) \\ E_m\epsilon_\theta &= \sigma_\theta - \nu_m(\sigma_r + \sigma_z). \end{aligned} \tag{3}$$

From (2), it is clear that the strains in the fiber, ϵ_r and ϵ_z, are measured from a stressed state such that the fiber just fits into the undeformed matrix, while the strains in the matrix in (3) are measured with respect to the unstressed state of the matrix.

Following earlier approaches, the fiber/matrix system is modeled by a cylindrical composite comprised of a fiber of radius R_f surrounded by the matrix with a circular cylindrical outer boundary of radius R such that the area fraction of the fiber is $\rho = (R_f/R)^2$ as depicted in Figs. 1 and 2. Two boundary conditions are considered on the outer cylindrical surface. Type I has zero normal and shear tractions, as is appropriate for experimental models with the same geometry. Type II boundary conditions have zero shear traction, σ_{rz}, on $r = R$ but with u_r constrained on $r = R$ to be everywhere equal to its value far above the debond crack front (i.e., $u_r^+(R)$). Far above the debond crack, $\sigma_r(R)$ is taken to be zero under the assumption that the only nonzero overall stress component is $\bar{\sigma}_z \equiv \bar{\sigma}$, thus determining $u_r^+(R)$. Type II conditions are intended to model a typical fiber/matrix cell in an aligned fiber reinforced matrix. The cylindrical model with Type II conditions is commonly used to approximate an array of fibers in a double periodic hexagonal arrangement. The approximate analysis of the models leads to relatively simple closed form formulas for all the basic results, although some of the nondimensional coefficients turn out to be rather lengthy expressions. Throughout the paper the approximate analysis will be compared with results

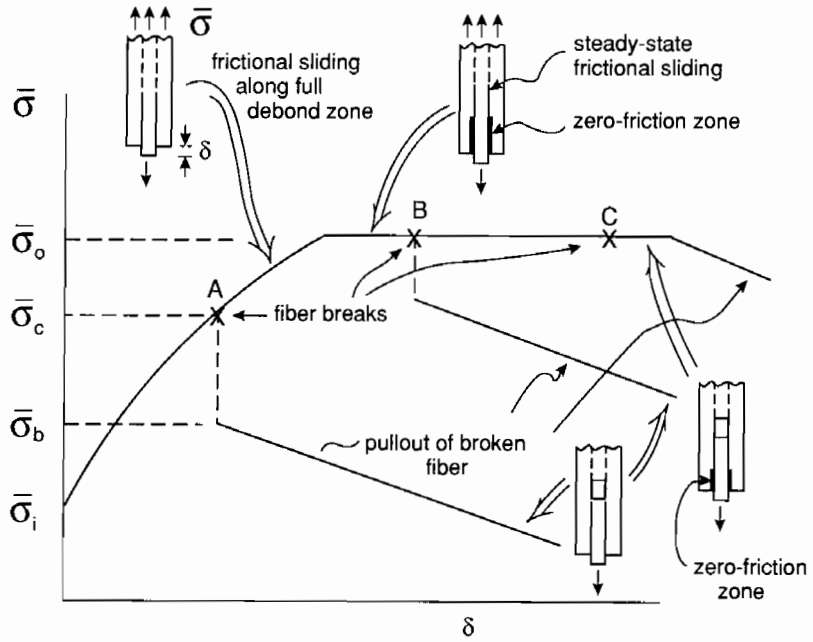

Fig. 3. Overall stress versus pullout displacement for constant friction case.

from an accurate numerical analysis of the models. Details of the numerical analysis are given in Appendix A.

Since there is a multitude of parameters characterizing the models and a variety of behaviors predicted depending on these parameters a synoptic overview will be presented in the remainder of this Introduction. The synopsis will be limited to systems where the fiber and matrix are both isotropic with the same modulus, E, and Poisson's ratio, ν, since most coefficients simplify considerably under these circumstances. It turns out that there is no difference in the models for the two types of boundary conditions when the fiber and the matrix have the same elastic properties, but some important differences emerge when there is a significant mismatch in the elastic properties. Following the Introduction, the sections are organized as follows: Section 2 – Basic results from the Lamé problem; Section 3 – Steady-state energy release rate in absence of friction and upper limit to interface toughness for mode 2 debonding; Section 4 – Debonding with constant friction; Section 5 – Debonding with Coulomb friction; Section 6 – Fiber Pullout with constant friction; Section 7 – Fiber Pullout with Coulomb friction. Appendix A – Numerical Analysis of Axisymmetric Model. Appendix B – Nondimensional Coefficients.

1.2. Synopsis for case of identical matrix and fiber properties

A sketch of overall stress $\bar{\sigma}$ as a function of the pullout displacement δ is shown in Fig. 3. This figure applies to the constant friction model, but the behavior for the Coulomb friction model is similar in most respects.

The steady-state energy release rate $\mathscr{G}$ for the mode 2 debond crack (the crack is assumed to be closed according to conditions discussed below) in the absence of friction is

$$\frac{\mathscr{G}}{ER_f} = \left[c_1 \frac{\bar{\sigma}}{E} + c_2 \epsilon^T\right]^2, \tag{4}$$

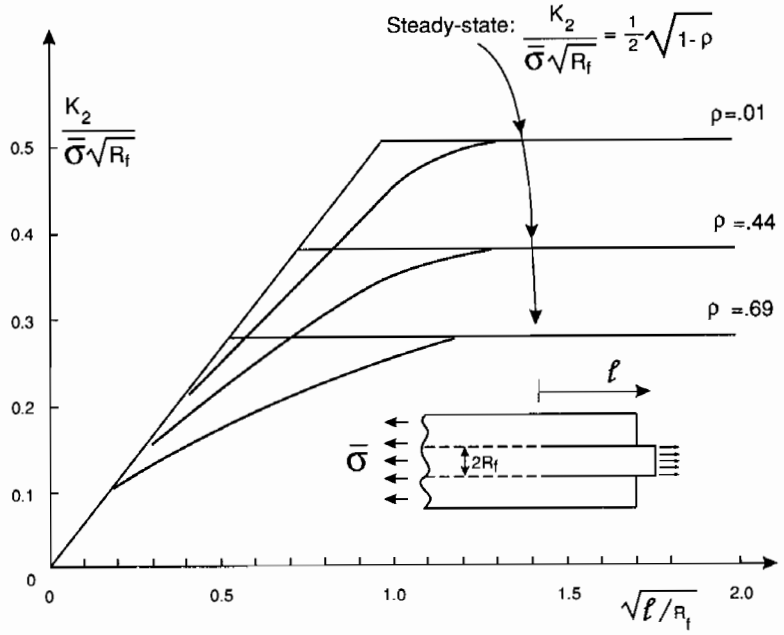

Fig. 4. Comparison between accurate numerical results (curved lines) and predictions of the model. Identical elastic properties of the fiber and matrix with $\nu = 0.2$. The surfaces of the fiber and matrix are free to slide over one another without friction and without loss of contact. $\mathcal{G} = (1-\nu^2)K_2^2/E$.

where

$$c_1 = \left[(1-\nu^2)(1-\rho)\right]^{1/2}/(2\rho) \quad c_2 = \tfrac{1}{2}\left[(1-\rho)/(1-\nu^2)\right]^{1/2}(1+\nu\lambda) \tag{5}$$ *

and where throughout the paper $\epsilon^T \equiv \epsilon_z^T$ and $\lambda \equiv \epsilon_r^T/\epsilon_z^T$. This is an exact result for a semi-infinite debond crack in an infinite cylinder. As mentioned above, the results in the synopsis apply to both sets of outer boundary conditions. Accurate numerical results (see Appendix A for solution details) for a crack of length l are shown in Fig. 4 for several ρ-values. The crack attains steady-state conditions, to a good approximation, when l equals the fiber radius.

No attempt will be made in the modeling to account for the behavior of the debond crack when l is smaller than about one fiber radius. It is assumed that the debond has been formed and is ready to propagate up the fiber. (In a fiber reinforced composite the main matrix crack might be expected to start the debond crack.) The "initiation" stress $\bar{\sigma}_i$ in Fig. 3 is the stress required to propagate the debond crack up the fiber. If $\mathcal{G}_c$ is the mode 2 toughness, measured by the critical value of the energy release rate, then by (4)

$$\frac{\bar{\sigma}_i}{E\epsilon^T} = \frac{1}{c_1}\left(\frac{\mathcal{G}_c}{ER_f\epsilon^{T2}}\right)^{1/2} - \frac{c_2}{c_1}. \tag{6}$$ *

The initiation stress $\bar{\sigma}_i$ can be negative if the nondimensional combination, $\mathcal{G}_c/(ER_f\epsilon^{T2})$ is sufficiently small. (In such cases, a finite length debond zone would be induced before any overall stress is applied.)

* An asterisk by an equation number indicates that it applies only to the case where the elastic properties of the fiber and matrix are identical.

Once the debond has initiated, as defined above, its length increases with increasing $\bar{\sigma}$ according to

$$l/R_f = \rho^{-1}(1-\rho)(\bar{\sigma}-\bar{\sigma}_i)/(2\tau) \quad (7)\ *$$

while the pullout displacement increases as

$$\frac{\delta}{R_f} = \frac{(1-\nu^2)}{\rho c_1}\left(\frac{\mathscr{G}}{ER_f}\right)^{1/2}\frac{l}{R_f} + \frac{(1-\nu^2)}{(1-\rho)}\frac{\tau}{E}\left(\frac{l}{R_f}\right)^2. \quad (8)\ *$$

Equations (7) and (8) apply either until the fiber breaks or until $\bar{\sigma}$ attains the value

$$\bar{\sigma}_0 = \rho E\epsilon_r^T/\nu \quad (9)\ *$$

This is the overall stress at which the compressive stress acting across the fiber/matrix interface vanishes at the bottom of the cylinder (i.e., at $z = l$) due to Poisson contraction of the fiber. This is the maximum value of overall stress which can be sustained. As depicted in Figs. 2 and 3, a steady-state is then attained where friction acts over a fixed zone of length l_0 below the debond crack front while the remaining zone below has $\sigma_r = 0$ across the interface with zero friction stress. Now l_0 is given by (7) with $\bar{\sigma} = \bar{\sigma}_0$. In steady-state the debond crack moves up the fiber at constant overall stress $\bar{\sigma}_0$ with δ/R_f given by (8) with $l = l_0$ plus an extra contribution

$$\left[\frac{(1-\nu^2)}{\rho}\frac{\bar{\sigma}_0}{E} + (1+\nu)\epsilon^T\right]\left(\frac{l-l_0}{R_f}\right)$$

Note that neither $\bar{\sigma}_i$ nor $\bar{\sigma}_0$ depends on the friction. Further, note that

$$\frac{\bar{\sigma}_0}{E\epsilon^T} - \frac{\bar{\sigma}_i}{E\epsilon^T} = \frac{\rho}{\nu} + \frac{c_2}{c_1} - \frac{1}{c_1}\left(\frac{\mathscr{G}_c}{ER_f\epsilon^{T2}}\right)^{1/2} \quad (10)\ *$$

It will later be shown that the condition for the debond crack to be closed below the tip (i.e., for a mode 2 interface crack) is $\bar{\sigma}_0 > \bar{\sigma}_i$. The maximum allowable value of the mode 2 toughness $\mathscr{G}_c^*$ consistent with mode 2 cracking is given by (10) with $\bar{\sigma}_i = \bar{\sigma}_0$, i.e.,

$$\frac{\mathscr{G}_c^*}{ER_f\epsilon^{T2}} = \left[\frac{c_1\rho}{\nu} + c_2\right]^2. \quad (11)\ *$$

If the mode 2 toughness exceeds $\mathscr{G}_c^*$ the debond crack will open all the way to the tip where mixed mode conditions will prevail. The present model is restricted to mode 2 debonding.

If the fiber breaks at $\bar{\sigma} = \bar{\sigma}_c$ on the rising portion of the pullout curve, such as at point A in Fig. 3, compression acts everywhere over the interface below the break. If l is the instantaneous length of the embedded portion of the fiber just after the break, then the associated overall stress $\bar{\sigma}_b$ is given by

$$\bar{\sigma}_b = 2\rho\tau l/R_f. \quad (12)$$

By (7), this is $\bar{\sigma}_b = (\bar{\sigma}_c - \bar{\sigma}_i)(1-\rho)$ if the fiber breaks at the debond crack tip. Following the break

$$d\bar{\sigma}/d\delta = 2\rho\tau/R_f. \quad (13)$$

The above formulas apply if the fiber breaks on the steady-state branch of the debond curve (i.e. at B in Fig. 3) as long as the embedded length of the broken fiber satisfies

$$l/R_f < \bar{\sigma}_0/(2\rho\tau). \quad (14)$$

If, however, the inequality in (14) is reversed, there will be a zone of zero compression at the bottom of the cylinder. Friction acts below the break over a length given by

$$l_0/R_f = \bar{\sigma}_0/(2\rho\tau). \tag{15}$$

No overall stress drop will occur when the fiber breaks, as depicted by point C in Fig. 3, until the embedded fiber length is reduced to l_0. Thereafter, (13) applies.

There is some confusion in the published literature on the appropriate displacement quantity for application of the stress–displacement relation to crack bridging calculations. The appropriate quantity, Δ, should be defined such that $\bar{\sigma}\,d\Delta$ is the *extra* work increment per unit area which occurs due to debonding and frictional sliding. Following the fiber break, $d\Delta = d\delta$ to a very good approximation; but prior to the break it will be shown later that

$$\Delta = (1-\rho)\delta \tag{16} *$$

for the case of common elastic properties of the fiber and matrix. Note that both δ and Δ differ by a factor of 2 from their usual definitions in crack bridging applications.

2. Basic results from the Lamé problem

The essential approximation made in the analysis of the models in the frictional sliding zone is that the axial and radial stresses in any section transverse to the z-axis are characterized by a Lamé problem given below. The approximation is valid as long as the axial stress in the fiber (and matrix) varies slowly over distances comparable to the fiber radius. Elementary equilibrium of the fiber below the debond tip in the axial direction gives

$$d\sigma_f/dz = (2/R_f)\tau, \tag{17}$$

where σ_f is the average axial stress in the fiber. It follows that validity of the approximation requires that τ be small compared to σ_f.

The stresses and strains *well above the debond* are given by the Lamé problem (see Fig. 5a) with the condition that $\epsilon_f = \epsilon_m$, together with continuity of normal stress, σ_r, and displacement across the fiber/matrix interface. In addition, the radial stress σ_r on the outer cylindrical surface at $r = R$ is zero. The relations needed are

$$\sigma_f^+ = a_1\bar{\sigma} - a_2 E_m \epsilon^T \tag{18a}$$

$$\sigma_r^+ = a_3\bar{\sigma} - a_4 E_m \epsilon^T \quad (\sigma_r \text{ at } r = R_f) \tag{18b}$$

$$\epsilon_f^+ = \epsilon_m^+ = a_5(\bar{\sigma}/E_m) + a_6\epsilon^T. \tag{18c}$$

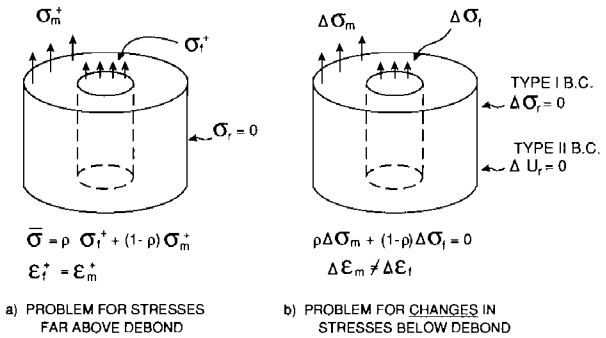

Fig. 5. Conventions for Lamé problems.

Unless otherwise stated, σ_r will denote the normal stress at the interface. The overall modulus for the bonded, composite cylinder is $\bar{E} \equiv d\bar{\sigma}/d\epsilon = E_m/a_5$. The a's are nondimensional and are functions of

$$\rho,\ \lambda \equiv \epsilon_r^T/\epsilon_z^T,\ E_f/E_m,\ \nu_f,\ \nu_m \text{ and } \zeta_f. \tag{19}$$

Explicit expressions for the a's and for the other coefficients arising later are given in Appendix B for two cases: (1) identical elastic properties of fiber and matrix and (2) an isotropic fiber with $\nu_f = \nu_m$ but with arbitrary E_f/E_m. Otherwise, a simple computer program can be written for computing all the coefficients, as prescribed in Appendix B. Note that $\epsilon^T \equiv \epsilon_z^T$; the effect of ϵ_r^T enters through the λ-dependence of a_2, a_4, and a_6.

The relations (18) reflect the feature of the Lamé solution that the axial stress and strain are uniform across the section in the matrix as well as the fiber. At any cross-section

$$\bar{\sigma} = \rho\sigma_f + (1-\rho)\sigma_m \tag{20}$$

since $\bar{\sigma}$ is by definition the average axial stress which is independent of z.

Let σ_f, σ_m, ϵ_f, etc. denote quantities below the debond crack tip, and let

$$\Delta\sigma_f = \sigma_f - \sigma_f^+, \quad \Delta\epsilon_f = \epsilon_f - \epsilon_f^+, \text{ etc.} \tag{21}$$

denote changes from values well above the debond front. The Lamé problem for the *changes* (see Fig. 5b) is governed by the stress–strain relations, (2) and (3), but with the mismatch strains deleted. Now, $\Delta\sigma_r$ and Δu_r are still continuous across the fiber–matrix interface at $r = R_f$, but there may be relative sliding so that $\Delta\epsilon_f \neq \Delta\epsilon_m$. In addition, overall equilibrium (20) requires $\rho\Delta\sigma_f + (1-\rho)\Delta\sigma_m = 0$. With $\Delta\sigma_f$ as the free variable in the solution (it will be related to τ in the models)

$$\Delta\sigma_m = \rho(1-\rho)^{-1}\Delta\sigma_f \tag{22a}$$

$$\Delta\sigma_r = b_1\Delta\sigma_f \quad (\Delta\sigma_r \text{ at } r = R_f) \tag{22b}$$

$$\Delta\epsilon_f = b_2\Delta\sigma_f/E_m \tag{22c}$$

$$\Delta\epsilon_m = -b_3\Delta\sigma_f/E_m, \tag{22d}$$

where the b's depend on the parameters in (19). There are two sets of b's (see Appendix B): for Type I conditions with $\Delta\sigma_r = 0$ on $r = R$ and for Type II conditions with $\Delta u_r = 0$ on $r = R$.

3. Steady-state energy release rate in absence of friction and upper limit to interface toughness for mode 2 debonding

Consider the geometry and loading in Fig. 6 where the debond crack is long and well away from either end of the cylinder. Suppose that the mismatch strains and applied stresses are such that $\sigma_r < 0$ across the interface below the debond and, further, suppose that frictionless sliding occurs. The energy release rate, $\mathcal{G}$, for the steady-state debond crack (a semi-infinite crack in an infinitely long cylinder) can be determined exactly and simply by evaluating the stored energy difference between sections well above and well below the debond crack tip, including the potential energy change of the applied loads, for a unit distance propagation of the crack. Expressions (23) apply to both sets of outer boundary conditions. The derivation of (23) for Type II conditions requires consideration of the fact that the potential energy of the applied loads is *not* twice the strain energy. Care must be taken to properly separate the contribution from the residual stress due to the mismatch strain. For later purposes, it is useful to consider a non-zero axial

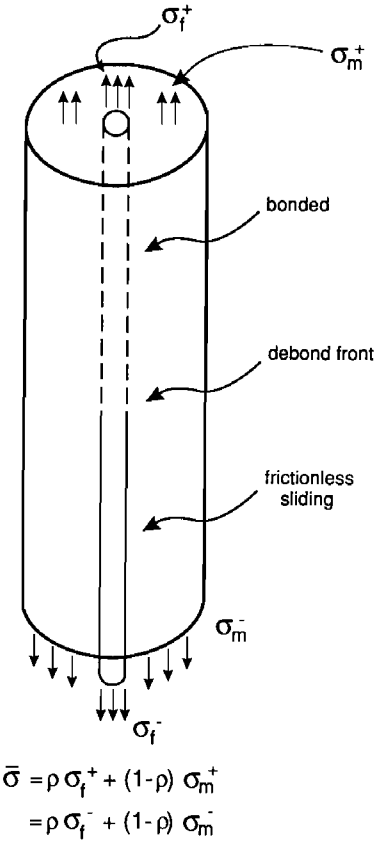

Fig. 6. Conventions for evaluating the steady-state energy release rate.

matrix stress σ_m^- below the debond as indicated in Fig. 6. The steady-state energy release rate is

$$\mathcal{G} = (R_f/E_m)\left[\rho(1-\rho)^{-1}c_1c_3(\sigma_f^- - \sigma_f^+)\right]^2 \tag{23a}$$

$$= (R_f/E_m)\left[c_1(\bar{\sigma} - c_3\sigma_m^-) + c_2E_m\epsilon^T\right]^2, \tag{23b}$$

where

$$c_1 = (2\rho)^{-1}(1-\rho a_1)(b_2+b_3)^{1/2}, \tag{24}$$

$$c_2 = \tfrac{1}{2}a_2(b_2+b_3)^{1/3} \quad c_3 = (1-\rho)/(1-\rho a_1).$$

For identical fiber and matrix elastic properties, the c's are the same for both types of boundary conditions and are given by (5) with $c_3 = 1$. For dissimilar properties, c_1 and c_2 depend on whether Type I or II conditions are in effect.

The form (23a) will be used below. It expresses the energy release rate in terms of the jump in the fiber stress from below to well above the debond crack tip. Note that (23a) is valid for the general case under consideration where $\epsilon^T \neq 0$ and $\sigma_m^- \neq 0$. Gao et al. (1988) have given an expression equivalent to $\mathcal{G} = (R_f/E_m)(c_1\bar{\sigma})^2$. We have verified that their expression for the equivalent of our c_1 is in complete agreement with the present results for the Type I boundary conditions, for which their modeling applies, for the case of the isotropic fiber with E_f and ν_f arbitrarily distinct from E_m and ν_m.

When the crack is closed below the debond, it is a mode 2 interface crack. The relation between the mode 2 stress intensity factor, K_2, and the energy release rate depends on the elastic properties of the fiber and matrix. If, for example, the fiber is isotropic and if the second Dundurs parameter, β, is zero (cf. Suo and Hutchinson, 1990), then

$$\mathcal{G} = \frac{1}{2}\left(\frac{1-\nu_f^2}{E_f} + \frac{1-\nu_m^2}{E_m}\right)K_2^2.$$

When the second Dundurs parameter does not vanish, or more generally for the case of an anisotropic fiber, when there exists an oscillatory-type singularity at the crack tip, the crack is no longer strictly in mode 2. Even so, the energy release rate expressions (23) still hold. Although we will regard the debond crack as a mode 2 interface crack, the models only require that a critical value of the energy release rate, $\mathcal{G}_c$, be maintained by the advancing debond crack.

The steady-state energy release rate is approached rapidly as the crack moves up from the end of the specimen as has already been discussed in connection with Fig. 4. The models use the steady-state expression for the energy release rate at all positions of the crack front in a way which is discussed later.

An important quantity in the models is the overall stress $\bar{\sigma}_0$ at which contact between the fiber and matrix is first lost at the bottom of the cylinder where $\sigma_m = 0$. Using (18a), (18b), (22b) with $\Delta\sigma_f = \bar{\sigma}/\rho - \sigma_f^+$, one obtains

$$\sigma_r = \left(a_3 + b_1\left(\rho^{-1} - a_1\right)\right)\bar{\sigma} - (a_4 - b_1 a_2)E_m\epsilon^T \tag{25a}$$

and, therefore, $\sigma_r = 0$ when

$$\bar{\sigma}_0 = \frac{(a_4 - b_1 a_2)E_m\epsilon^T}{\left(a_3 + b_1\left(\rho^{-1} - a_1\right)\right)}. \tag{25b}$$

For Type I boundary conditions, a direct elementary calculation gives

$$\bar{\sigma}_0 = \rho E_f \epsilon_r^T/\nu_f. \tag{26a}$$

For Type II boundary conditions the formula for $\bar{\sigma}_0$ is not a simple combination of the parameters; thus let

$$\bar{\sigma}_0 = c_4\rho E_f \epsilon_r^T/\nu_f, \tag{26b}$$

where by (25b)

$$c_4 = \frac{\nu_f E_m}{\rho\lambda E_f}\frac{(a_4 - b_1 a_2)}{\left(a_3 + b_1\left(\rho^{-1} - a_1\right)\right)}. \tag{26c}$$

For Type I conditions $\bar{\sigma}_0$ is always positive. For Type II boundary conditions $\bar{\sigma}_0$ can be negative for certain combinations of fiber and matrix properties. When the fiber and matrix properties are identical, $c_4 = 1$ and $\bar{\sigma}_0 > 0$; but when ν_f is sufficiently small compared to ν_m and/or E_f is sufficiently large compared to E_m, c_4 can be negative. Using the results in Appendix B for the Type II conditions with $\nu_f = \nu_m$, one can show that b_1 becomes negative as E_f/E_m increases; then by (26c) since $a_3 = 0$, $c_4 \to \infty$ as b_1 becomes zero and $c_4 < 0$ with $b_1 < 0$. By (22b), a system with $b_1 < 0$ has the property that the compressive stress on the fiber/matrix interface *increases* with distance below the debond front and is greatest at the bottom of the cylinder. We suspect that such systems will not be particularly effective for fiber reinforced matrix composites, but that issue deserves closer consideration. Recall that Type II conditions model fibers in a composite, while Type I applies to the single fiber/cylinder configuration.

In summary, coefficients b_1 and c_4 are the most sensitive to whether Type I or II conditions are invoked ($c_4 \equiv 1$ for Type I). Moreover, both play important roles, as will be seen below. In the remainder of this paper we will focus on systems for which $b_1 > 0$ and $c_4 > 0$ and thus $\bar{\sigma}_0 > 0$. Some of the results below are insensitive to the signs of these quantities, but others are not.

Assuming $\bar{\sigma}_0$ is positive, there exists a mode 2 interface toughness $\mathcal{G}_c^*$ such that for $\mathcal{G}_c > \mathcal{G}_c^*$ there will be no contact between fiber and matrix anywhere below the debond when the crack is advancing. If $\mathcal{G}_c > \mathcal{G}_c^*$ the assumptions underlying the model will no longer be in effect. To obtain this upper limit to the toughness, identify $\mathcal{G}$ with $\mathcal{G}_c^*$ in (23b) with $\bar{\sigma} = \bar{\sigma}_0$ and $\sigma_m^- = 0$ to obtain

$$\mathcal{G}_c^* = (R_f/E_m)\left[c_1\bar{\sigma}_0 + c_2 E_m \epsilon^T\right]^2 \tag{27a}$$

or, by (26b),

$$\frac{\mathcal{G}_c^*}{E_m R_f \epsilon^{T2}} = \left[c_1 c_4 \rho \frac{E_f}{E_m}\frac{\lambda}{\nu_f} + c_2\right]^2. \tag{27b}$$

Thus, if $\mathcal{G}_c = \mathcal{G}_c^*$, the debond crack would propagate up the fiber at $\bar{\sigma} = \bar{\sigma}_0$ with no friction since $\sigma_r = 0$ at the interface everywhere below the crack tip. If $\mathcal{G}_c > \mathcal{G}_c^*$, the crack would necessarily be open below the tip, and mixed mode conditions would pertain. Charalambides and Evans (1989) have considered mixed mode fiber debonding for conditions when the debond crack is open below the tip.

4. Debonding with constant friction

In this section the friction stress between the fiber and matrix is taken to be a constant value, τ, where $\sigma_r > 0$ and zero where $\sigma_r = 0$. From this point onward, a symbol decorated with $(\,)^-$ denotes its value just below the debond crack tip. Below the tip the average stress in the fiber varies according to (17) so that for $0 < z < l_0$ (cf. Fig. 2)

$$\sigma_f = \sigma_f^- + 2\tau(z/R_f) \tag{28}$$

while

$$\sigma_m = \sigma_m^- - 2\rho(1-\rho)^{-1}\tau(z/R_f). \tag{29}$$

If the zero-friction zone shown in Fig. 2 exists (i.e. if $\bar{\sigma} = \bar{\sigma}_0$), then $\sigma_f = \bar{\sigma}/\rho$ and $\sigma_m = 0$ for $l_0 < z < l$. When $\bar{\sigma} < \bar{\sigma}_0$, then $l \equiv l_0$ and $\sigma_f = \bar{\sigma}/\rho$ and $\sigma_m = 0$ at $z = l_0$. In either case,

$$l_0/R_f = (\bar{\sigma}/\rho - \sigma_f^-)/(2\tau) \tag{30}$$

To determine σ_f^- (and thus σ_m^-), we impose the fracture condition $\mathcal{G} = \mathcal{G}_c$ at the debond crack tip using (23a) to obtain

$$\sigma_f^- = \sigma_f^+ + \frac{(1-\rho)}{\rho}\frac{1}{c_1 c_3}\left(\frac{E_m \mathcal{G}_c}{R_f}\right)^{1/2} \tag{31}$$

where σ_f^+ is given by (18a).

In the absence of friction (31) provides the exact jump in the average fiber stress from well above the tip to just below the tip when the debond crack is in steady-state. Friction will primarily affect the distribution in the stress in the fiber *below* the tip as reflected by (28). The jump condition (31) in the presence of friction will have an error of order τ/σ_f^- since only the friction within about one fiber radius of the tip is not treated accurately by the steady-state relation. (Thus a "load" of order $2\pi R_f^2 \tau$ on the fiber is

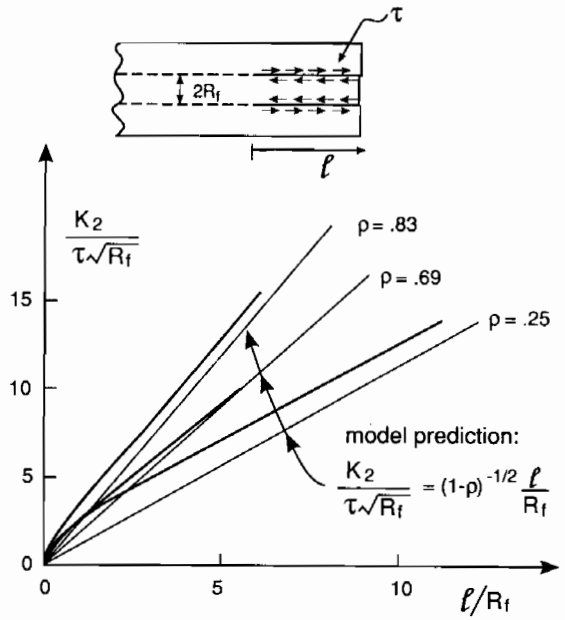

Fig. 7. Comparison of accurate numerical results (curved lines) with model prediction for friction contribution to K_2. Identical elastic properties of fiber and matrix with $\nu = 0.2$. The surfaces of the fiber and matrix have equal and opposite constant shear stress τ applied to them. The surfaces are constrained to remain in normal contact.

inadequately modeled compared with the load $\pi R_f^2 \sigma_f^-$.) The accuracy of the approximation is illustrated in Fig. 7 for a system with identical elastic properties of the fiber and matrix. Figure 7 isolates the effect of friction loading. The fiber and matrix surfaces as loaded by a uniform shear stress τ and are free to slide but not to lose contact; $\bar{\sigma} = 0$ and $\epsilon_z^T = \epsilon_r^T = 0$. The variation of K_2 is shown as calculated by the full numerical method described in Appendix A. Also shown is the present approximation obtained using (23a), i.e.,

$$K_2/\left(\tau R_f^{1/2}\right) = (1-\rho)^{-1/2}(l/R_f). \tag{32}$$

Figure 7 demonstrates that the approximation becomes increasingly accurate as l/R_f increases. It has already been noted in connection with Fig. 4 that, in the absence of friction with $\bar{\sigma} \neq 0$, the energy release rate, or equivalently K_2, approaches the steady-state value when l/R_f is about unity. Since the full problem for K_2 is a linear superposition of results such as those in Figs. 4 and 7, it follows that (23a) and the jump condition (31) are good approximations in the presence of friction once l exceeds 2 or 3 times R_f. This assumes σ_f^- is regarded as the average fiber stress just below the debond tip.

Let $\bar{\sigma}_i$ denote the overall stress level at which the debond crack begins to progress up the fiber. As discussed earlier, it is assumed that an initiating flaw on the order of R_f in length is already present. With $\sigma_f^- = \bar{\sigma}_i/\rho$ in (31) and with σ_f^+ given by (18a), one obtains

$$\frac{\bar{\sigma}_i}{E_m \epsilon^T} = \frac{1}{c_1}\left(\frac{\mathcal{G}_c}{E_m R_f \epsilon^{T2}}\right)^{1/2} - \frac{c_2}{c_1}, \tag{33}$$

where the expression for c_3 has been used along with the identity

$$(1-\rho)c_2 = \rho c_1 c_3 a_2. \tag{34}$$

Similar manipulations show that (30) can be re-expressed as

$$l/R_f = \rho^{-1}(1-\rho)(\bar{\sigma}-\bar{\sigma}_i)/(2c_3\tau). \tag{35}$$

The debond region $0 \le z \le l$ increases linearly with $\bar{\sigma}-\bar{\sigma}_i$ until the condition $\sigma_r = 0$ is reached at the lower end of the fiber/matrix interface at $z = l$. This condition occurs when $\bar{\sigma} = \bar{\sigma}_0$, where $\bar{\sigma}_0$ is given by (26). Thereafter, the length of the region of the debond over which $\sigma_r < 0$, and thus over which friction acts, has *fixed* length l_0 given by (35) with $\bar{\sigma} = \bar{\sigma}_0$. Once $\bar{\sigma}$ attains $\bar{\sigma}_0$, the debond moves up the fiber at constant overall stress with a region in which $\sigma_r = 0$ (and no friction) of increasing length $l - l_0$, as depicted in Fig. 3. It is readily shown that the condition $\mathcal{G}_c < \mathcal{G}_c^*$ required for a mode 2 debond crack is equivalent to $\bar{\sigma}_i < \bar{\sigma}_0$, assuming $\bar{\sigma}_0 > 0$. In fact, the two pairs of quantities are related by

$$c_1(\bar{\sigma}_0 - \bar{\sigma}_i) = (E_m\mathcal{G}_c^*/R_f)^{1/2} - (E_m\mathcal{G}_c/R_f)^{1/2}. \tag{36}$$

Formulas for the displacement difference δ between the end of the fiber and the matrix (see Fig. 2) and for the additional displacement Δ with arises from debonding are readily derived. First, the displacement difference from the model is defined as

$$\delta = \int_0^l (\epsilon_f - \epsilon_m)\,dz = \int_0^l (b_2+b_3)(\Delta\sigma_f/E_m)\,dz$$

$$= (b_2+b_3)\left\{\frac{(1-\rho)}{\rho c_1 c_3}\left(\frac{\mathcal{G}_c}{E_m R_f}\right)^{1/2} l_0 + \frac{\tau l_0^2}{E_m R_f} + \left[(\rho^{-1}-a_1)\bar{\sigma}_0/E_m + a_2\epsilon^T\right](l-l_0)\right\}. \tag{37}$$

For $\bar{\sigma} < \bar{\sigma}_0$, $l \equiv l_0$ and is given by (35). For $\bar{\sigma} = \bar{\sigma}_0$, l_0 is given by (35) but $l - l_0$ (or δ) can be regarded as a free parameter which increases monotonically.

The additional displacement Δ due to debonding is the displacement difference at the lower end of the fiber between the specimen with and without debonding. It is this quantity (and *not* δ) which should be

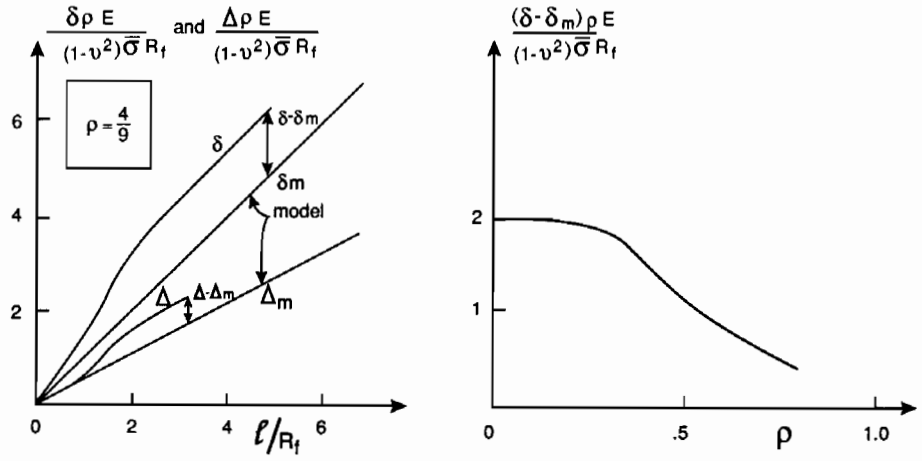

Fig. 8. Fiber pullout δ and additional displacement due to debonding Δ versus l/R_f for the case of identical elastic properties of the matrix and fiber with $\nu = 0.2$. The system is subject to overall stress $\bar{\sigma}$ with no friction or residual stresses. The surfaces are constrained to remain in normal contact across the interface. The curved lines are the accurate numerical results. The curve on the right shows the contribution omitted by the curved model for debond lengths greater than about 2Rf.

taken as the half-separation distance between the crack faces in a bridging model. Since the strain difference in the fiber, with and without debonding is $\epsilon_f - \epsilon_f^+$, it follows that

$$\Delta = \int_0^l (\epsilon_f - \epsilon_f^+)\, dz = b_2 \int_0^l (\Delta\sigma_f/E_m)\, dz = (b_2/(b_2 + b_3))\delta, \tag{38}$$

which reduces to (16) for identical fiber/matrix properties.

A comparison between predictions for δ and Δ from the full numerical analysis and those from the model are shown in Fig. 8. The comparisons, which focus just on the effect of the overall loading $\bar{\sigma}$, reveal that the model prediction becomes increasingly accurate as the debond length grows, but fails to account for a "crack-like" contribution which is independent of debond length when l/R_f exceeds about 2. This extra contribution to δ is plotted as a function of ρ on the right in Fig. 8. In principle, the extra contributions to δ and Δ could be added to (37) and (38), but the *relative* effect decreases as l/R_f increases and should not be of much significance when l/R_f has exceeded about 5. Also omitted from (38) is the contribution to Δ due to the matrix crack alone when $l = 0$. This contribution also becomes relatively small as l/R_f increases.

5. Debonding with coulomb friction

The overall stress at which the debond begins to advance up the fiber (assuming the existence of an initial flaw) is $\bar{\sigma}_i$ in (33), and the relation between the fiber stress just below the debond tip and the stress state well above the tip is still given by (31). This latter result, together with (18b) and (22b), gives the normal stress acting across the interface just below the debond tip:

$$\sigma_r^- = a_3\bar{\sigma} - a_4 E_m \epsilon^T + \frac{b_1}{c_1 c_3}\frac{(1-\rho)}{\rho}\left(\frac{E_m \mathscr{G}_c}{R_f}\right)^{1/2}. \tag{39}$$

Recalling that $\sigma_r^- = 0$ when $\bar{\sigma} = \bar{\sigma}_0$ and $\mathscr{G}_c = \mathscr{G}_c^*$, one can then rewrite (39) using (36) as

$$\sigma_r^- = -\rho^{-1}(1-\rho)(b_1/c_3)\left[\bar{\sigma}_0 - \bar{\sigma}_i + k_1(\bar{\sigma}_0 - \bar{\sigma})\right] \tag{40}$$

where

$$k_1 = \rho(1-\rho)^{-1} a_3 c_3 / b_1. \tag{41}$$

In Appendix B it is seen that $a_3 = 0$ when the fiber is isotropic with $\nu_f = \nu_m$ for arbitrary E_f/E_m, and thus $k_1 = 0$ for this case. In the discussion which follows it will be assumed that σ_r^- is compressive. If for Type II conditions b_1 is negative, one should proceed from (39) without introducing $\bar{\sigma}_i$. This is not pursued here.

With σ_r as the normal stress across the interface at any point below the debond tip, the friction stress is taken to be

$$\tau = -\mu\sigma_r \tag{42}$$

assuming $\sigma_r \le 0$. Using (17) and (22b) one obtains

$$\frac{d\Delta\sigma_f}{dz} = -\frac{2\mu}{R_f}(\sigma_r^+ + b_1\Delta\sigma_f). \tag{43}$$

The solution to (43), subject to (31) at $z = 0$ with (39), is

$$\Delta\sigma_f \equiv \sigma_f - \sigma_f^+ = \frac{1-\rho}{\rho}\frac{1}{c_1 c_3}\sqrt{\frac{E_m \mathscr{G}_c}{R_f}} - \frac{\sigma_r^-}{b_1}[1 - e^{-\zeta}], \tag{44}$$

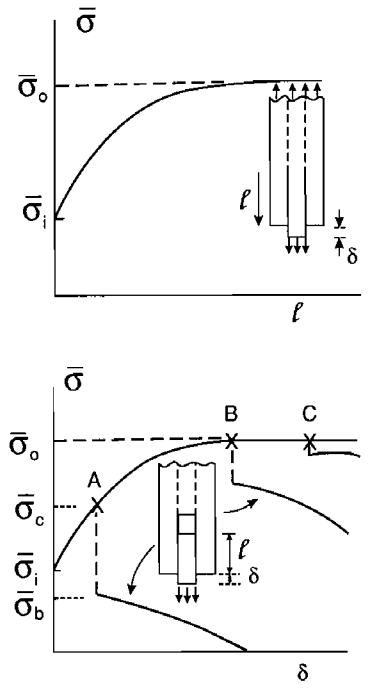

Fig. 9. Overall stress versus debond length and pullout displacement for the Coulomb friction case.

where

$$\zeta = 2\mu b_1 z/R_f. \tag{45}$$

Then using (22b) and (39) again, one finds

$$\sigma_r = \sigma_r^- \, e^{-\zeta}. \tag{46}$$

The solution has the required property that the sliding is one-signed, consistent with the direction of the friction stress. In addition, from (46) it is immediately noted that σ_r is everywhere negative below the debond tip if σ_r^- is negative.

The length of the debond region can be found from (44) noting that $\sigma_f = \bar{\sigma}/\rho$ at $z = l$. After some algebraic manipulation, one finds

$$\frac{l}{R_f} = \frac{1}{2\mu b_1} \ln\left[\frac{\bar{\sigma}_0 - \bar{\sigma}_i + k_1(\bar{\sigma}_i - \bar{\sigma})}{\bar{\sigma}_0 - \bar{\sigma}}\right], \tag{47}$$

where k_1 is given by (41). A sketch of this relation is shown in Fig. 9. Note that quasi steady-state behavior, similar to that for the constant friction case, is achieved when the debond has attained the length (using $\zeta = 3$ in (45))

$$l/R_f \cong 3/(2\mu b_1). \tag{48}$$

This becomes $l/R_f \cong 3/(\mu\nu)$ for identical properties for the fiber and matrix. Once this level of debond has been achieved, the overall stress has nearly attained its limit $\bar{\sigma}_0$. As the debond advances further up the fiber, the zone where most of the friction stress acts is of length $3/(2\mu b_1)$ below the tip.

Finally, the opening displacement δ and the additional displacement Δ can be calculated using their definitions in (37) and (38), together with (44). The results are

$$\delta = ((b_2 + b_3)/b_2)\Delta$$
$$= (b_2 + b_3)\left\{ \frac{1-\rho}{\rho} \frac{l}{c_1 c_3} \left(\frac{\mathscr{G}_c}{E_m R_f} \right)^{1/2} - \frac{R_f \sigma_r^-}{2\mu b_1^2 E_m} \left[e^{-\zeta_l} + \zeta_l - 1 \right] \right\}, \tag{49}$$

where $\zeta_l = 2\mu b_1 l/R_f$. A sketch of the relation between δ and $\bar{\sigma}$ is also shown in Fig. 9.

The present analysis is similar in a number of respects to that of Gao et al. (1988). These authors considered the Coulomb friction problem with Type I boundary conditions. As in the present approach, debonding is controlled by a critical value of the energy release rate. In their study the initial state of stress in the fiber is one of compressive radial stress with no axial prestress. Thus their analysis is applied to the special case considered here where ϵ_r^T and ϵ_z^T are such that $\sigma_z = 0$ in the unloaded bonded fiber. It should be noted that the axial prestress in the fiber makes a significant contribution to the energy release rate. Gao et al. identify quantities equivalent to $\bar{\sigma}_i$ and $\bar{\sigma}_0$, and derive an expression for the smallest value of initial compression across the interface consistent with mode 2 debonding.

6. Fiber pullout with constant friction

As depicted in Fig. 3, let $\bar{\sigma}_c$ be the overall stress at which the fiber breaks and let $\bar{\sigma}_b$ be the overall stress just following the break before any additional pullout has occurred. There are two possibilities which must be considered: (i) $\sigma_r < 0$ everywhere below the break and (ii) a zone of friction with $\sigma_r < 0$ extending only part way towards the end of the cylinder with a second friction-free zone in which $\sigma_r = 0$ above the end.

If $\bar{\sigma}_c < \bar{\sigma}_0$, full contact over the debond region occurs after the break, and (12) applies. From (35), the debond length at fiber fracture is

$$l/R_f = \rho^{-1}(1-\rho)(\bar{\sigma}_c - \bar{\sigma}_i)/(2c_3\tau). \tag{50}$$

Thus, if the break occurs at the debond tip,

$$\bar{\sigma}_b = 2\rho\tau(l/R_f) = (1-\rho)(\bar{\sigma}_c - \bar{\sigma}_i)/c_3 \tag{51}$$

Then during pullout

$$\frac{d\bar{\sigma}}{d\delta} \cong -\frac{d\bar{\sigma}}{dl} = -\frac{2\rho\tau}{R_f}. \tag{52}$$

If $\bar{\sigma}_c = \bar{\sigma}_0$, the two possibilities mentioned above must be considered. Let l be the length of the fiber below the break at the instant of fracture. If $2\rho\tau l/R_f < \bar{\sigma}_0$, then friction will act over the full zone below the break and

$$\bar{\sigma}_b = 2\rho\tau l/R_f \tag{53}$$

Equation (52) will apply during pullout. If, however, $2\rho\tau l/R_f > \bar{\sigma}_0$, there will be a zone of friction of length

$$l_b = \bar{\sigma}_0 R_f/(2\rho\tau), \tag{54}$$

which does not extend all the way to the end of the cylinder. In this case $\bar{\sigma}_b = \bar{\sigma}_0$ and the overall stress remains at $\bar{\sigma}_0$ until the length l_b of the broken fiber remains in the matrix. Beyond that point, the overall stress drops according to (52). The two possibilities are indicated by breaks at B and C in Fig. 3.

7. Fiber pullout with coulomb friction

Equation (43) continues to apply after the fiber breaks except that now σ_f must vanish at the break and thus the condition at $z = 0$ (the top of the break) is $\Delta\sigma_f = -\sigma_f^+$. The solution to (43) gives

$$\sigma_f = -\left(\sigma_r^b/b_1\right)[1 - e^{-\zeta}] \quad \sigma_r = \sigma_r^b\, e^{-\zeta}. \tag{55}$$

Here σ_r^b is the normal stress across the interface at the top of the broken fiber:

$$\begin{aligned}\sigma_r^b &= \sigma_r^+ + b_1\Delta\sigma_f = \sigma_r^+ - b_1\sigma_f^+ \\ &= -(a_1b_1 - a_3)\bar{\sigma} - (a_4 - b_1b_2)E_m\epsilon^T \qquad (56)\\ &= -\frac{\nu}{2}\bar{\sigma} - \frac{\lambda}{2}(1-\rho)E\epsilon^T, \qquad (56a)\ *\end{aligned}$$

where (56a) only applies for the case of identical elastic properties for the fiber and matrix. A further reduction of the expression for σ_r^b can be obtained using the equation for the *unbroken* fiber stating that $\sigma_r = 0$ when $\bar{\sigma} = \bar{\sigma}_0$ and $\sigma_m = 0$. Combining this later equation with (56) gives

$$\sigma_r^b = -b_1\bar{\sigma}_0/\rho - (a_1b_1 - a_3)(\bar{\sigma} - \bar{\sigma}_0). \tag{57}$$

Since $\sigma_f = \bar{\sigma}/\rho$ at $z = l$, (55) gives

$$\bar{\sigma} = -\left(\rho\sigma_r^b/b_1\right)[1 - e^{-\zeta_l}], \tag{58}$$

where $\zeta_l = 2\mu b_1 l/R_f$. This relation holds as the fiber is pulled out where l is the current length of the fiber remaining in the matrix. Using (57) in (58) and solving for $\bar{\sigma}/\bar{\sigma}_0$, one finds

$$\frac{\bar{\sigma}}{\bar{\sigma}_0} = \frac{(1-k_2)(1-e^{\zeta_l})}{1 - k_2(1 - e^{-\zeta_l})}, \tag{59}$$

where

$$k_2 = \rho\left(a_1 - (a_3/b_1)\right). \tag{60}$$

For an isotropic fiber with $\nu_f = \nu_m$, $k_2 = \rho E_f/(\rho E_f + (1-\rho)E_m))$.

If the fiber breaks such that $\zeta_l \gg 1$ (i.e., $l/R_f > 3/(2\mu b_1)$, say, with $\bar{\sigma}_c \cong \bar{\sigma}_0$), then $\bar{\sigma}_b \cong \bar{\sigma}_0$. There is only a small drop in $\bar{\sigma}$ associated with fiber fracture, as at point C in Fig. 9, and the overall stress remains near $\bar{\sigma}_0$ until l/R_f decreases to a length of about $3/(2\mu b_1)$. On the other hand, if the fiber breaks when $\bar{\sigma}_b < \bar{\sigma}_0$, the overall stress experiences a sudden drop with fiber fracture and immediately begins to fall with pullout, as illustrated by the breaks at A and B in Fig. 9. From (59), the slope of the pullout curve after fiber fracture is

$$\frac{d\bar{\sigma}}{d\delta} = -\frac{d\bar{\sigma}}{dl} = -\frac{2\mu b_1\bar{\sigma}_0}{R_f}\,\frac{(1-k_2)\,e^{-\zeta_l}}{\left[1 - k_2(1 - e^{-\zeta_l})\right]^2}, \tag{61}$$

which approaches a constant value, $-2\mu b_1\bar{\sigma}_0(1-k_2)/R_f$, as $l \to 0$.

Acknowledgement

This work was supported in part by DARPA University Research Initiative (Subagreement PO #VB38639-0 with the University of California, Santa Barbara, ONR Prime Contract N00014-86-K0753),

the National Science Foundation (Grant MSM-88-12779) and the Division of Applied Sciences, Harvard University.

References

Bright, J.B., D.K. Shetty, C.W. Griffin and S.Y. Limaye (1989), Interfacial bonding and friction in silicon carbide (filament)-reinforced ceramic- and glass-matrix composites, *J. Am. Ceram. Soc. 72*, 1891–1898.

Charalambides, P.G. and A.G. Evans (1989), Debonding properties of residually stressed brittle-matrix composites, *J. Am. Ceram. Soc. 72*, 746–753.

Evans, A.G. (1989), The mechanical performance of fiber-reinforced ceramic matrix composites, *Mat. Sci. Eng. A107*, 227–239.

Gao, Y-C., Y-W. Mai and B. Cotterell (1988), Fracture of fiber reinforced materials, *J. Appl. Math. and Phys. (ZAMP) 39*, 550–572.

Marshall, D.B. and W.C. Oliver (1987), Measurement of interfacial mechanical properties in fiber-reinforced ceramic composites, *J. Am. Ceram. Soc. 70*, 542–548.

Rice, J.R. (1968), Mathematical analysis of fracture, in: H. Leibowitz, ed., *Fracture, an Advanced Treatise*, Vol. II, Academic Press, NY, pp. 191–311.

Sigl, L.S. and A.G. Evans (1989), Effects of residual stress and frictional sliding on cracking and pullout in brittle matrix composites, *Mech. Materials 8*, 1–12.

Suo, Z. and J.W. Hutchinson (1990), Interface crack between two elastic layers, *Int. J. Fracture 43*, 1–18.

Thouless, M.D., A.G. Evans, M.F. Ashby and J.W. Hutchinson (1987), The edge cracking and spalling of brittle plates, *Acta Metall. 35*, 1333–1341.

Thouless, M.D., O. Sbaizers, L.S. Sigl and A.G. Evans (1989), Effect of interface mechanical properties on pullout in a SiC-fiber-reinforced lithium aluminum silicate glass-ceramic, *J. Am. Ceram. Soc. 72*, 525–532.

Wells, J.F.K. and P.W.R. Beaumont (1985), Crack-tip energy absorption processes in fibre composites, *J. Mater. Sci. 20*, 2735–2749.

Appendix A. Numerical analysis of axisymmetric model

The full numerical method used to solve the several problems presented in the body of the paper is discussed briefly in the following. More details will be published elsewhere. The method is based on the use of a continuous distribution of dislocations in an integral equation formulation to replicate the crack (Rice, 1968). The relevant dislocation solution for the semi-infinite cylinder cannot be obtained in closed form, and a new feature to the present solution method is the use of the finite element method to obtain all but the singular part of the desired dislocation solution. Thus, the dislocation solution which forms the kernel of the integral equation is represented by its known singular part times an additional nonsingular contribution which is obtained using the finite element method. The nonsingular portion of the kernel is fit to the functional representation and thus is obtained "once and for all". Thereafter, standard solution procedures for solving integral equations, such as those employed by Thouless et al. (1987) and Suo and Hutchinson (1990) for plane strain problems, can be used to solve the various cases.

The Green's function $u(z, \xi)$ and $v(z, \xi)$ that denote surface displacements at position z following a point force at position ξ (see Fig. 10) are found for both the fiber and the matrix by the finite element method. When u and v denote radial and axial displacements, superscripts $(\ )^{\mathrm{F}}$ and $(\ )^{\mathrm{M}}$ refer to the fiber surface and matrix surface, and subscripts $(\ )_{\mathrm{P}}$ and $(\ )_{\mathrm{Q}}$ refer to displacements due to normal and shear tractions, the following eight functions are represented numerically: $u_{\mathrm{P}}^{\mathrm{F}}$, $u_{\mathrm{Q}}^{\mathrm{F}}$, $v_{\mathrm{P}}^{\mathrm{F}}$, $v_{\mathrm{Q}}^{\mathrm{F}}$, $u_{\mathrm{P}}^{\mathrm{M}}$, $u_{\mathrm{Q}}^{\mathrm{M}}$, $v_{\mathrm{P}}^{\mathrm{M}}$ and $v_{\mathrm{Q}}^{\mathrm{M}}$.

For a given variation of normal and shear tractions $\sigma(\xi)$ and $\tau(\xi)$ the surface displacements are given by expressions such as

$$u^{\mathrm{F}}(z) = \int_{\text{interface}} \left\{ u_{\mathrm{P}}^{\mathrm{F}}(z, \xi)\sigma(\xi) + u_{\mathrm{Q}}^{\mathrm{F}}(z, \xi)\tau(\xi) \right\} \mathrm{d}\xi. \tag{A1}$$

Inversely, for a given variation of displacements across the interface, the corresponding $\sigma(\xi)$ and $\tau(\xi)$ can be determined.

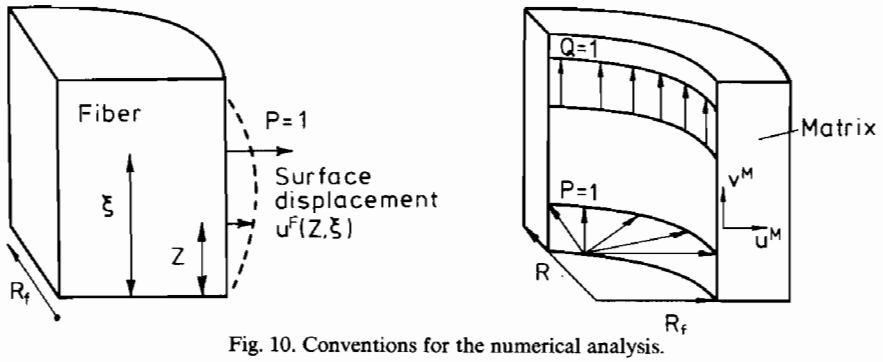

Fig. 10. Conventions for the numerical analysis.

The stress variation caused by a dislocation at position z_d at the interface is found by imposing the following boundary conditions

$$u^F(z) - u^M(z) = 0 \tag{A2}$$

$$v^F(z) - v^M(z) = \begin{cases} 0, & z \geq z_d \\ b, & z \leq z_d. \end{cases} \tag{A3}$$

At the same time equilibrium requires

$$\begin{aligned} \tau^F(z) + \tau^M(z) &= 0 \\ \sigma^F(z) + \sigma^M(z) &= 0. \end{aligned} \tag{A4}$$

Close to the dislocation origin at z_d, plane strain conditions exist and the stress field is

$$\sigma_{rz}(z) = cb/(z - z_d), \tag{A5}$$

where $c = \bar{E}_m \bar{E}_f/(2\pi(\bar{E}_m + \bar{E}_f))$ and $\bar{E} = E/(1-\nu^2)$ (Suo and Hutchinson, 1990). Here attention is restricted to the case of an isotropic fiber and it is assumed that the second Dundurs elastic mismatch parameter, β, is zero. The finite element method is used to generate the solution for the dislocation in the cylindrical geometry. That solution, with the correct singularity built-in, supplies the kernel functions for the integral equation as described below.

The accuracy of the FEM representation of the dislocation stress is illustrated in Fig. 11. For R_f/R near unity, plane strain conditions hold for the solution sufficiently near the dislocation. The plane strain solution for a dislocation a distance h below a free surface is (Thouless et al., 1987)

$$\sigma_{rz} = \frac{cb}{x}\left[1 - \frac{4x^2}{4+x^2} + \frac{8x^2}{(4+x^2)^2} + \frac{4(x^4 - 12x^2)}{(x^3 - 12x)^2 + (8 - 6x^2)^2}\right], \tag{A6}$$

for the case where the elastic mismatch vanishes with $x = (z - z_d)/h$. Shown in Fig. 11 is the numerical solution for the cylindrical geometry with $R_f/R = 10/11$ along with the distribution from (A6).

It is useful to have an analytical approximation for the stress in the dislocation solution when one solves the integral equation. Two functional approximations were considered:

$$\sigma_{rz}(z, z_d) = cb(z - z_d)^{-1} F(z, z_d) \tag{A7}$$

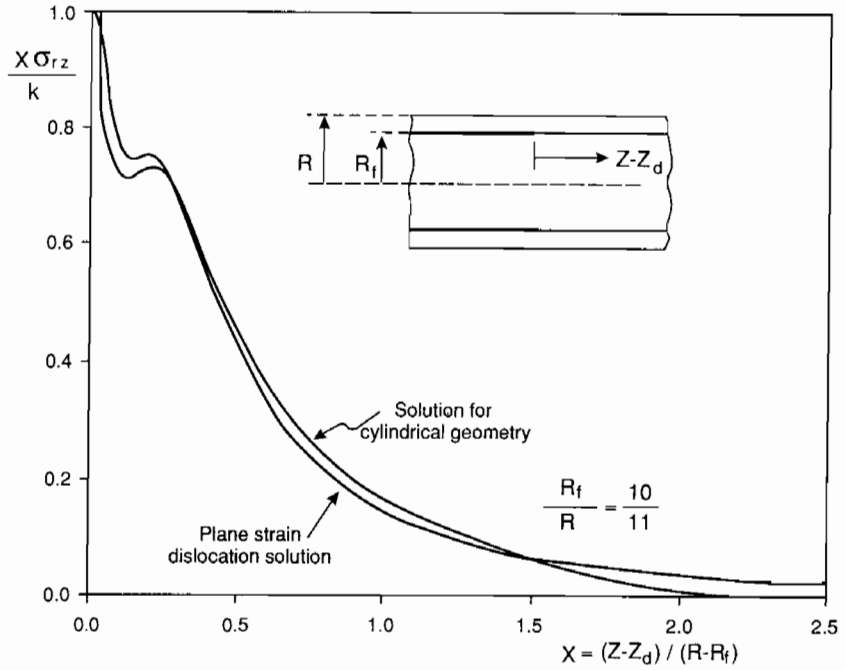

Fig. 11. Comparison of FEM representation of dislocation stress distribution in the cylindrical configuration with the plane strain distribution for a dislocation located beneath a free surface.

where, with $\eta = z - z_d$,

$$F(z, z_d) = 1 + a_1|\eta| + b_1\eta^2 \quad |\eta| \le \eta_c$$
$$= 0 \quad |\eta| > \eta_c \tag{A8}$$

or

$$F(z, z_d) = (1 + a_2|\eta|)(1 + b_2|\eta|^s)^{-1}. \tag{A9}$$

For a given location z_d of the dislocation the free parameters a_1, b_1 and η_c or a_2, b_2 and s were chosen to fit the numerically generated solution. Thus the free parameters depend on the distance of the dislocation from the bottom of the cylinder. The results for the energy release rate shown in Fig. 4 were found to be only weakly dependent on small variations in these free parameters, which indicates that a highly accurate representation of F in (A7) is not very critical.

After the results for F have been generated, the solution procedure follows along the lines as in Thouless et al. (1987). With reference to Fig. 12, make the change of variable

$$z_d = \frac{(t-1)R_f}{(1 + 2R_f/L + t)} \quad -1 \le t \le 1 \tag{A10}$$

so that the shear stress along the interface due to a continuous distribution of dislocations $a(t) \equiv b(z_d)$ is

$$\sigma_{rz}(z) = \int_{-1}^{1} c(u-t)^{-1} G(u, t)(\mathrm{d}z_d/\mathrm{d}t)a(t)\,\mathrm{d}t, \tag{A11}$$

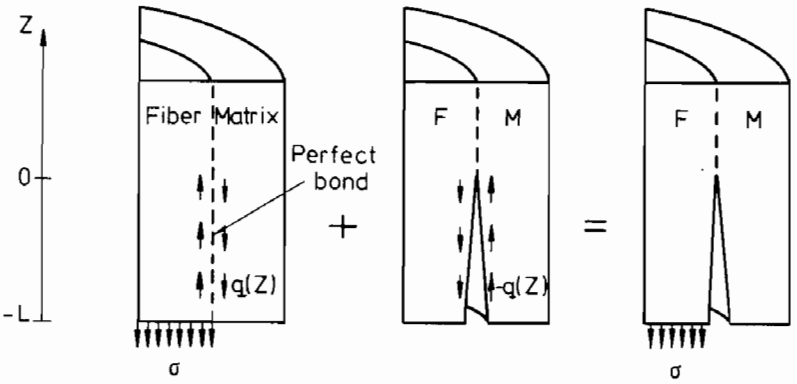

Fig. 12. Geometry and loadings for integral equations formulation.

where $G(u, t) \equiv F(z, z_d)$ and where z and u are related in the same manner as z_d and t in (A10). The stress from (A11) is used to cancel the stress from a calculation with perfect bonding, as depicted in Fig. 12. Friction stresses may be included by simple superposition. In (A11), $a(t)$ is represented by Chebyshev polynomials. Standard solution procedures are employed as described in Thouless et al. (1987).

Appendix B. Nondimensional coefficients

B.1. Coefficients for state far above debond crack tip

Continuity of u_r and σ_r at $r = R_f$ require

$$C\begin{bmatrix} \sigma_m/E_m \\ \epsilon_z \end{bmatrix} = A\begin{bmatrix} \sigma_f/E_m \\ \epsilon_z \end{bmatrix} + B\begin{bmatrix} \epsilon_r^T \\ \epsilon_z^T \end{bmatrix}, \tag{B1}$$

where

$$\begin{aligned} c_{11} &= (1+\nu_m)(1+\rho(1-2\nu_m))/(2\nu_m\rho) & c_{21} &= -(1-\rho)/(2\nu_m\rho) \\ c_{12} &= -(1+\nu_m+\rho(1-\nu_m))/(2\nu_m\rho) & c_{22} &= -c_{21} \\ a_{11} &= (\zeta_f - 2\nu_f^2)E_m/(2\nu_f E_f) & a_{21} &= 1/(2\nu_f) \\ a_{12} &= -\zeta_f/(2\nu_f) & a_{22} &= -E_f/(2\nu_f E_m) \\ b_{11} &= 1,\ b_{21} = 0,\ b_{12} = \zeta_f/(2\nu_f) & b_{22} &= E_f/(2\nu_f E_m). \end{aligned}$$

The stress acting across the interface is

$$\sigma_r = a_{21}\sigma_f + a_{22}E_m\epsilon^T + b_{22}E_m\epsilon^T. \tag{B2}$$

Using (20) and writing ϵ_r^T as $\lambda\epsilon_z^T$ with $\epsilon^T \equiv \epsilon_z^T$, one obtains

$$H\begin{bmatrix} \sigma_f/E_m \\ \epsilon_z \end{bmatrix} = \frac{\bar{\sigma}}{E_m}\begin{bmatrix} -c_{11}/(1-\rho) \\ -c_{21}/(1-\rho) \end{bmatrix} + \epsilon^T\begin{bmatrix} \lambda + b_{12} \\ b_{22} \end{bmatrix}, \tag{B3}$$

where

$$h_{11} = -\rho(1-\rho)^{-1}c_{11} - a_{11} \quad h_{21} = -\rho(1-\rho)^{-1}c_{21} - a_{21}$$
$$h_{12} = c_{12} - a_{12} \quad h_{22} = c_{22} - a_{22}.$$

Then, based on their definitions in (18), the a's are obtained as

$$\begin{bmatrix} a_1 \\ a_5 \end{bmatrix} = -(1-\rho)^{-1}H^{-1}\begin{bmatrix} c_{11} \\ c_{21} \end{bmatrix} \quad \begin{bmatrix} -a_2 \\ a_6 \end{bmatrix} = H^{-1}\begin{bmatrix} \lambda + b_{12} \\ b_{22} \end{bmatrix} \tag{B4}$$
$$a_3 = a_{21}a_1 + a_{22}a_5 \quad a_4 = a_{21}a_2 - a_{22}a_6 - b_{22}.$$

B.2. Coefficients for state changes below debond crack tip

B.2.1. Type I boundary conditions

Continuity of u_r and σ_r at $r = R_f$, together with $\sigma_r = 0$ on $r = R$ both above and below the crack tip require

$$C\begin{bmatrix} \Delta\sigma_m/E_m \\ \Delta\epsilon_m \end{bmatrix} = A\begin{bmatrix} \Delta\sigma_f/E_m \\ \Delta\epsilon_f \end{bmatrix}, \tag{B5}$$

where the coefficients of C and A are given above. By (22a),

$$M\begin{bmatrix} \Delta\epsilon_f \\ \Delta\epsilon_m \end{bmatrix} = \frac{\Delta\sigma_f}{E_m}\begin{bmatrix} \rho(1-\rho)^{-1}c_{11} + a_{11} \\ \rho(1-\rho)^{-1}c_{21} + a_{21} \end{bmatrix}, \tag{B6}$$

where $M_{11} = -a_{12}$, $M_{12} = c_{12}$, $M_{21} = -a_{22}$ and $M_{22} = c_{22}$. Thus, by (22),

$$\begin{bmatrix} b_2 \\ -b_3 \end{bmatrix} = M^{-1}\begin{bmatrix} \rho(1-\rho)^{-1}c_{11} + a_{11} \\ \rho(1-\rho)^{-1}c_{21} + a_{21} \end{bmatrix} \tag{B7}$$

Since $\Delta\sigma_r = a_{21}\Delta\sigma_f + a_{22}\Delta\epsilon_f E_m$,

$$b_1 = a_{21} + a_{22}b_2. \tag{B8}$$

B.2.2. Type II boundary conditions

The constrained boundary condition (see Fig. 1) requires $\Delta u_r = 0$ at $r = R$. This condition, together with continuity of σ_r and u_r at $r = R_f$, requires that (B5) hold where A is unchanged but now the coefficients of C are

$$c_{11} = -(1-\rho)(1+\nu_m)(1-2\nu_m)/(2\nu_m\rho) \quad c_{21} = (\rho + 1 - 2\nu_m)/(2\nu_m\rho)$$
$$c_{12} = (1-\rho)(1-\nu_m)/(2\nu_m\rho)$$
$$c_{22} = \left(\nu_m - (1-\nu_m)\left(1 + (1-2\nu_m)\rho^{-1}\right)(2\nu_m)^{-1}\right)/\left((1+\nu_m)(1-2\nu_m)\right).$$

Equation (B6) holds with the components of M determined from the new c_{ij}. The coefficients, b_1, b_2 and b_3, are again given by (B7) and (B8).

B3. Coefficients for case of identical elastic properties of fiber and matrix

$$a_1 = 1, \quad a_2 = (1-\rho)(1+\nu\lambda)/(1-\nu^2), \quad a_3 = 0,$$
$$a_4 = \tfrac{1}{2}(1-\rho)(\lambda+\nu)/(1-\nu^2), \quad a_5 = 1, \quad a_6 = \rho \tag{B9}$$
$$b_1 = \tfrac{1}{2}\nu, \quad b_2 = 1-\nu^2, \quad b_3 = \rho(1-\nu^2)/(1-\rho).$$

The above b's apply to both types of boundary conditions on the outer surface of the cylinder. Coefficients c_1 and c_2 are given by (5) (with $c_3 = 1$ and $c_4 = 1$) and these also apply to both sets of boundary conditions.

B.4. Coefficients for isotropic fiber with $\nu_f = \nu_m \equiv \nu$

$$a_1 = \frac{E_f}{\bar{E}} \quad a_2 = \frac{(1-\rho)E_f}{(1+\nu)\big(E_f + (1-2\nu)\bar{E}\big)}\big(2\nu\lambda + 1 - \nu + (1+\nu)\big(E_f/\bar{E}\big)\big)$$
$$a_3 = 0 \quad a_4 = \frac{(1-\rho)E_f(\lambda+\nu)}{(1+\nu)\big(E_f + (1-2\nu)\bar{E}\big)} \quad a_5 = \frac{E_m}{\bar{E}} \quad a_6 = \rho\frac{E_f}{\bar{E}}.$$

where $\bar{E} = \rho E_f + (1-\rho)E_m$ is the overall modulus of the bonded system.

B.4.1. Type I boundary conditions

$$b_1 = \frac{\nu\bar{E}}{(1+\nu)E_f + (1-\nu)\bar{E}} \quad b_2 = \frac{(1+\nu)E_m\big(E_f + (1-2\nu)\bar{E}\big)}{E_f\big((1+\nu)E_f + (1-\nu)\bar{E}\big)}$$
$$b_3 = \frac{\rho(1+\nu)\big(E_f + (1-2\nu)\bar{E}\big)}{(1-\rho)\big((1+\nu)E_f + (1-\nu)\bar{E}\big)}$$
$$c_1^2 = \frac{(1+\nu)(1-\rho)E_m^2\big(E_f + (1-2\nu)\bar{E}\big)}{4\rho^2\bar{E}E_f\big((1+\nu)E_f + (1-\nu)\bar{E}\big)} \quad c_3 = \frac{\bar{E}}{E_m}$$
$$c_2^2 = \frac{1}{4}\frac{(1-\rho)E_f\big((1+\nu)E_f + (1-\nu)\bar{E}\big)}{(1+\nu)\bar{E}\big((1-2\nu)\bar{E} + E_f\big)}\left[1 + \frac{2\nu\lambda\bar{E}}{(1+\nu)E_f + (1-\nu)\bar{E}}\right]^2.$$

B.4.2. Type II boundary conditions

$$b_1 = \frac{\{(1-\nu^2)E^* + (1-\nu)^2E_m - (1+\nu)[2(1-\nu)^2E_f + (1-2\nu)(1-\nu+\rho(1+\nu))(E_m - E_f)]\}}{2\nu(1-\nu)[(1+\nu)E^* + (1-\nu)E_m]}$$
$$b_2 = \frac{(1+\nu)E_m\{2(1-\nu)^2E_f + (1-2\nu)[1-\nu+\rho(1+\nu)](E_m - E_f)\}}{(1-\nu)E_f[(1+\nu)E^* + (1-\nu)E_m]}$$
$$b_3 = \frac{\rho(1+\nu)\{(1-\rho)(1+\nu)(1-2\nu)(E_f - E_m) + 2(1-\nu)^2E_m\}}{(1-\nu)(1-\rho)[(1+\nu)E^* + (1-\nu)E_m]},$$

where $E^* = \rho E_m + (1-\rho)E_f$. The coefficients c_1 and c_2 can be evaluated using the general relations (24) and c_4 by (26c); the explicit expressions are too lengthy to be useful. Coefficient c_3 is the same as in Type I.

B.5. Coefficients for transversely isotropic fiber

When $\nu_f \neq \nu_m$ and $\zeta_f \neq 1 - \nu_f$, the expressions for the various coefficients are extremely lengthy and unrevealing. For such cases it is recommended that a simple computer program be written based on (B1) through (B8). A copy of such a program can be obtained from the first author.